ATMOSPHERIC FLOW

Experimental Parametric Study of the Influence of an Idealized Upstream Ridge on the Flow Characteristics over Alaiz Mountain

Boris Conan

Environmental and Applied Fluid Dynamics Department, von Karman Institute for Fluid Dynamics, Belgium, boris.conan@vki.ac.be

Supervisor: Jeroen van Beeck

Professor, Environmental and Applied Fluid Dynamics Department, von Karman Institute for Fluid Dynamics, Belgium, vanbeeck@vki.ac.be

University Supervisor: Sandrine Aubrun

HDR, PRISME Laboratory, Polytech'Orléans, France, sandrine.aubrun@univ-orleans.fr

Abstract

This paper presents a preliminary quantification of the influence of an upstream obstacle on the top of a main topography. Its influence is compared to the effect of changing inlet terrain roughness conditions. A simplified 2D model is built and several inlet conditions are coupled with different upstream relief distances. The velocity deficit and the turbulence increase are discussed. The main result is the higher influence of the inlet conditions compared to the obstacle position.

Keywords: atmospheric boundary layer, wind resource asessment, complex terrain, PIV, Alaiz hill.

1. Introduction

Physical modeling in a wind tunnel is a common tool for numerous applications like atmospheric dispersion investigations, wind comfort assessment or wind loads on buildings studies. In the booming wind energy sector, wind tunnel tests can be a suitable tool for the assessment of the wind resource, especially for wind turbine micro-siting in complex terrain.

The simulation of atmospheric flows in the wind tunnel requires the verification of a number of assumptions. Taking as implicit the similarity criteria (dimensionless numbers) described by Cermak [1], a certain number of parameters have to be taken into account: the Reynolds number dependence, the modelling of the local roughness on the mock-up, the reproduction of inflow conditions and the choice of the modelled area.

The latter is a major parameter that drives the choice of the scaling factor and influences all the other parameters. The choice of the area to model is the result of a compromise between: having a large area in order to reproduce closely the effects of the surroundings topographies, the limitation of the wind tunnel dimensions (blockage) and the difficulties to reproduce realistic flows at very high scaling factors (model roughness, reproduction of inflow conditions, measurements limitations).

The Alaiz site (Fig. 1) tested in the wind tunnel [2] illustrates this conflict. The terrain is a 1130m high mountain situated next to Pamplona (Spain); it is a very complex terrain stretching over 10km in the W-E direction and 8km in the N-S direction [3]. When the wind comes from the North, one of the dominant directions, it faces a ridge before reaching the mountain (position x = 0.75m in Fig. 1). The ridge is around 1/3 of the main mountain's height and 7km upstream. An influence is expected, it is then chosen to include it in the wind tunnel mock-up. Giving the test section size (2m x 3m), that leads to a very large scaling factor of 1/5300.

Experimental tests are realized at the von Karman Institute in the 2m x 3m x 15m wind engineering test section. Particle Image Velocimetry and hot-wire anemometry measurements are performed along a 2D plane parallel to the wind direction as described in Figure 1.

One of the main results of this study is the high influence of the upstream ridge on the flow field on the main mountain. Figure 1 shows the Fractional Speed-up Ratio (FSR) over the terrain and enlightens the important speed-down (almost -50% compared to the inlet conditions R1) at the foot of the mountain (R2) due to the disturbance of the upstream ridge (x = 0.75m). Measurements show the speed-up and the turbulence intensity at the top of the mountain very affected by the separation occurring at the ridge. It leads to the conclusion that the area of influence of the flow up to the mountain is vast and must be taken into account in the model.
On the other hand, the extreme scaling factor leads to some difficulties in reproducing the inflow conditions. The inlet turbulence profile provided by the VDI guidelines [4] is hard to match close to the surface for this scaling factor. Additionally, questions emerge concerning the relaxation of the Reynolds number and the surface roughness of the model.

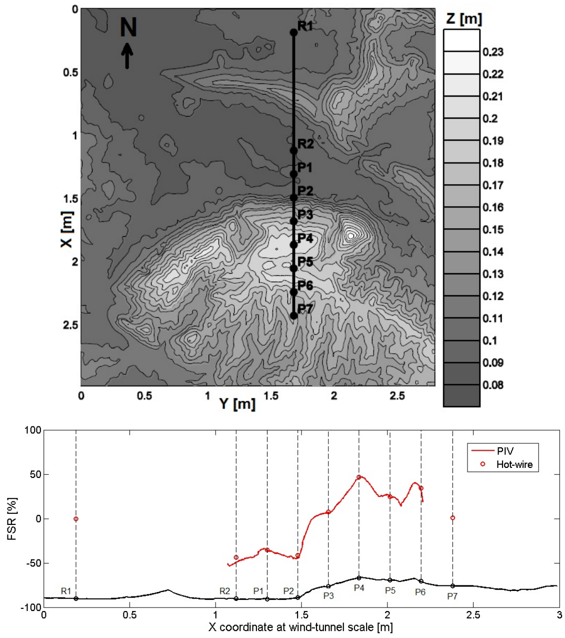

Figure 1: Top view of the Alaiz terrain at the wind tunnel scale 1/5300 (top). Fractionnal Speed-up Ratio (FSR) at 90m over the mountain (bottom).

Very high scales are difficult to work with, however, as shown by the study of the Alaiz mountain, the flow field over a mountain is influenced by an upstream ridge three times smaller and situated 7km upstream.

This study aims at illustrating the question of the modelled area size through a parametric study designed to evaluate the influence of an upstream hill on a major downstream mountain. Different configurations will be tested by changing the distance from the ridge to the mountain and inlet conditions.

2. Experimental conditions

2.1. Experimental set-up

For the parametric study, a suction-type wind tunnel is used with a 0.35m x 0.35m x 2m test section. The velocity can be adjusted up to 35 m/s. The use of a reduced size tunnel is an advantage for a parametric study so that several configurations can be tested in a short time and for limited costs.
To keep the blockage ratio below 10%, the model is scaled down to 1/19200. At that scale, the simulation of turbulence scales might not be respected. The objective of this model is a parametric study; results may not be used for direct application at full scale.
The mock-up is a two-dimensional model of the width of the test section representing the line shown in Figure 1 from point R1 to P7. The choice of a two dimensional model is supported by the comparison performed in a previous study showing a good agreement between the wind tunnel test and a 2D CFD computation on this very same line [5]. The front ridge is simplified to a triangular shape and can be displaced upstream and downstream for the parametric study. In the original configuration: H = 2.5*h; D = 24*h and h = 13 mm (Fig. 2). The wind tunnel is equipped for two-dimensional Particle Image Velocimetry (PIV) measurements. Three planes are necessary to measure all the topography but a reconstruction of the measurements is possible for average quantities: U, V, I_u and I_v. 500 images are acquired and averaged for each plane.

2.2. Flow conditions

The atmospheric inflow conditions are modeled thanks to a 1m fetch where roughness generators are placed to simulate an atmospheric boundary layer (ABL). Three different inlet conditions (Fig. 3) are tested in the wind tunnel by combining surface roughness (lego floor with $h_{lego-floor}$ = 2mm) and Counihan wings (h_{CW} = 90mm) in the following, they are named: FP = Flate plate, LF = Lego floor and CW = Counihan wings + Lego floor. (Fig. 3)
At the scale of 1/19200, the boundary layers represent three different terrain roughness (Fig. 3) from slightly rough to rough according to the VDI guidelines [4].

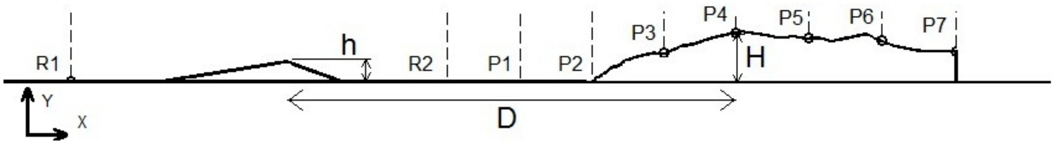

Figure 2: Mock-up in the wind tunnel.

The two-dimensionality of the flow is estimated by performing PIV planes at four locations in the Z direction around the middle measurement plane. In a +/- 20mm slice in the middle of the test section the velocity varies by less than 0.7% and the turbulence by less than 0.4%.
In the range of the wind tunnel velocities, measurements at three different Reynolds number are recorded at the top of the model. Taking as reference length the front ridge height (h), it gives Re = 8300; Re = 12400 and Re = 16600. The Reynolds number dependency decreases with increasing velocity, the maximum discrepancies are at around h = 400 m with less than 3% difference in speed. The very high scaling factor may explain this dependency. The highest velocity (20 m/s) is chosen for the tests.

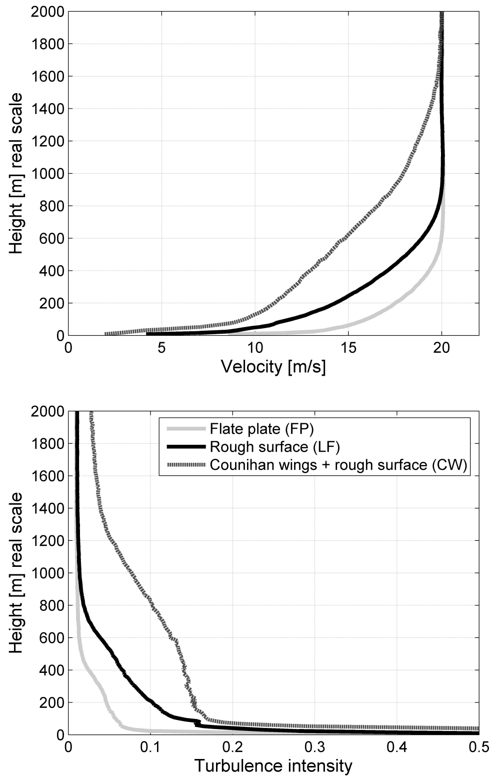

Figure 3: Boundary layer simulated in the test section.

3. Presentation of the results

3.1. Flow around the original configuration

When it reaches the front ridge, the velocity increases and creates an over-speed at its top. On the lee side, the flow separates and creates a recirculation bubble (Fig. 4). This separation is generating high turbulence and a very important velocity reduction at the height of the ridge. The velocity recovers after the perturbation but the flow is still disturbed, with lower velocities and higher turbulence, when it reaches the mountain. The behavior is very similar to the one described on the three-dimensional model [2].
Two local quantities are used in this study: the Fractional Speed-up Ratio (FSR) and the Turbulence Intensity Ratio (TIR), they represent the ratio of change compare to the inlet conditions:

$$FSR_i = \frac{U_i - U_{inlet}}{U_{inlet}} \tag{1}$$

$$TIR_i = \frac{Ti_i - Ti_{inlet}}{Ti_{inlet}} \tag{2}$$

The FSR is computed at 90m and compared with the study at scale 1/5357 presented in the introduction. It illustrates well the behavior of the flow around the ridge and the mountain (Fig. 5), the front ridge creates a speed-up followed by a strong speed-down in the recirculation, then the speed increases again until x = 1.25m, at this point the mountain creates a speed-down. On the mountain, the speed is rising until the top, where the speed-up is the highest. The mountain speed-up is nearly 100% front the foot to the top but due to the front ridge, it is reduced to around 50%.

Figure 5 shows the comparison between the test in the big wind tunnel at scale 1/5 357 with a three-dimensional model and the test presented above at 1/19 000 scale with a two-dimensional model. The two measurements are very comparable, both in terms of behavior (shape) and quantities; the speed-up at the top of the mountain is very well reproduced. Discrep-

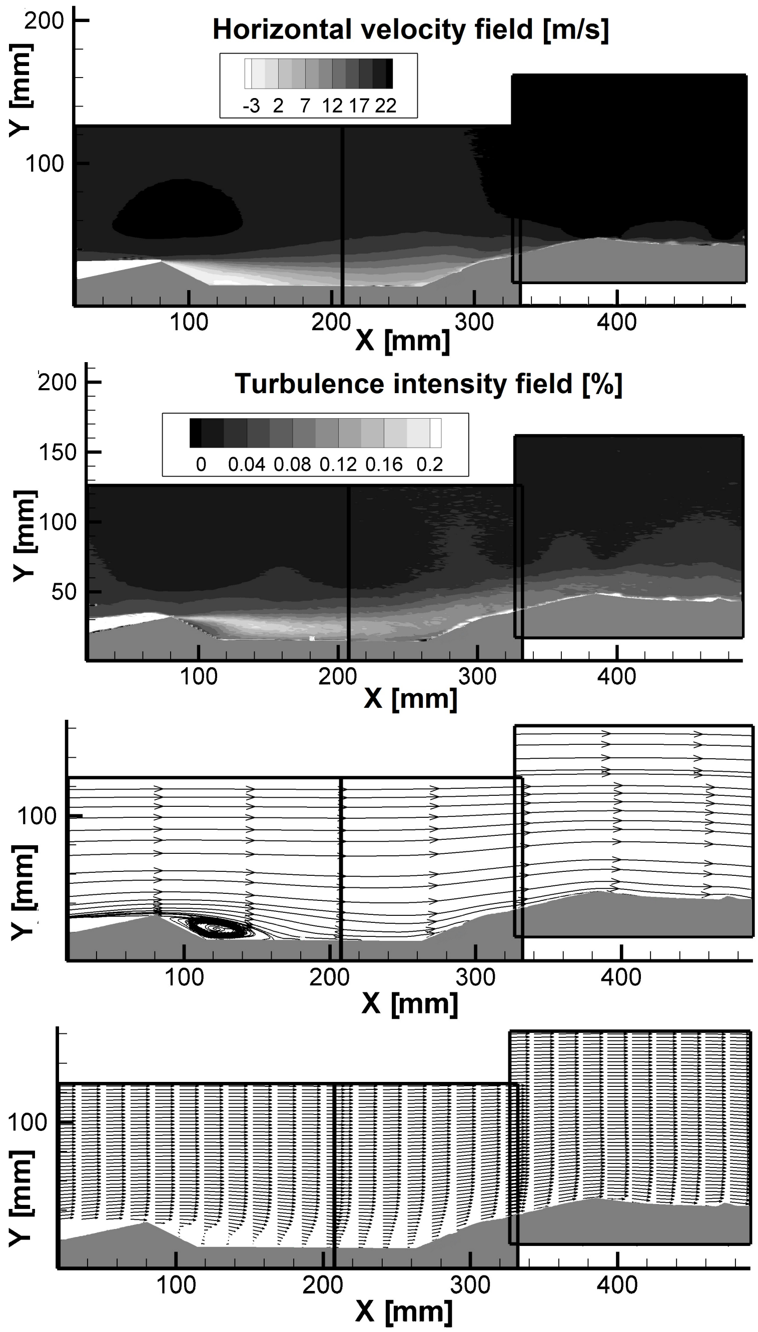

Figure 4: Velocity and turbulence intensity fields, velocity streamlines and velocity vector field in the original Alaiz configuration with low roughness inlet conditions (FP).

ancies appear in the recirculation after the ridge (x = 0.75m), this is most probably due to the simplification of the geometry (2D), therefore, 3D effects are not all reproduced. The two dimensionality of the flow in the measurement plane was already detected by the comparison of the wind tunnel tests with 2D CFD computation [5] and reinforces the validity of the choice of a two-dimensional model.

3.2. *Profiles at the top of the mountain (position P4)*

Figure 6 presents the results (PIV) from the parametric study with 5 ridge positions and three inlet

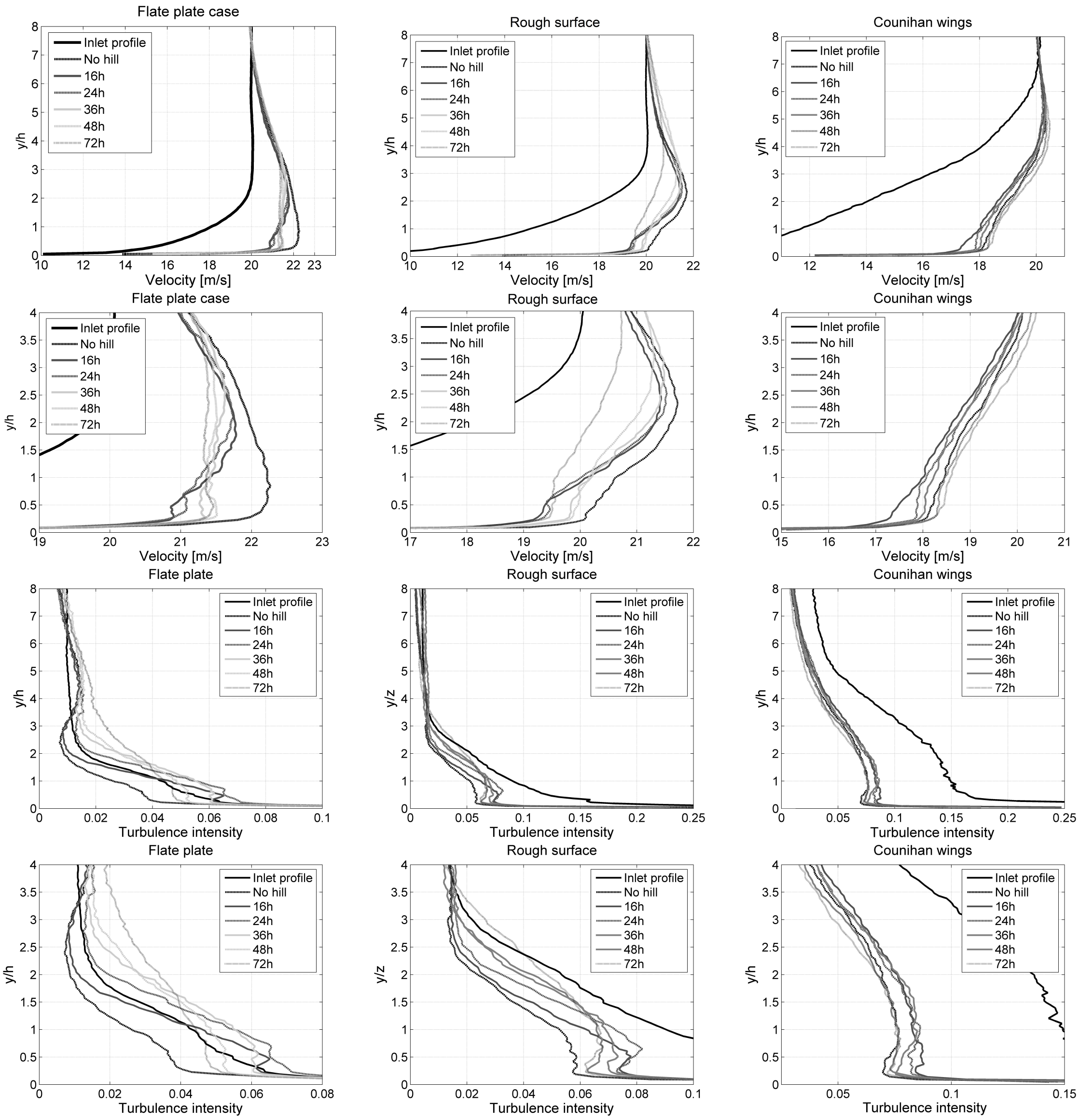

Figure 6: Velocity and turbulence profiles for five ridge distances: 16h, 24h, 36h, 48h and 72h, and three inlet conditions: left: ”flate plate” (FP), middle: ”rough surface” (LF) and right: ”Counihan wings + rough surface” (CW). Global views and clser look are proposed.

conditions (see section 2.2).

Two heights (a.l.g) are defined to describe the influence of the ridge on the flow at the top of the mountain: z = 2h and z = h/2.
The influence of the ridge is clearly enlightened by comparing the velocity profile for the ”no ridge” case with any of the ridge distances: the velocity is reduced and the turbulence increased at, below and above the ridge’s height. Concerning the Counihan wings case, the boundary layer is not completely measured in the PIV field so the normalization of the velocity profile can be a problem: the velocity of the ”no ridge” case might be underestimated.

Figure 7 presents the ratio of change in velocity and in turbulence intensity with the distance downstream of the ridge; the reference point is the case without front ridge. This is a great tool to describe the relative evolution of the values with the distance.

The effect of the ridge distance depends of the height of comparison, at z = h/2, for all inlet condi-

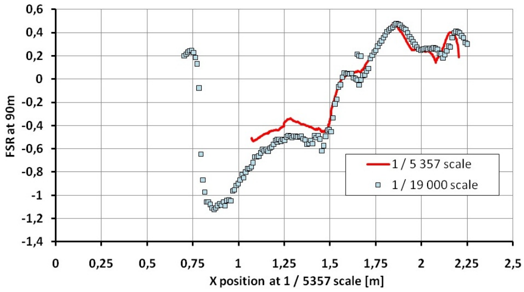

Figure 5: Comparison of the FSR at two scales.

tions, the velocity deficit, that is very high after the separation, gradually decreases with increasing distance. In the same time, the turbulence intensity decreases. It can be noticed from Figure 7 that the ratio of velocity is increasing equally for the flat-plate (FP) and the rough surface (LF) cases. With the Counihan wings, (CW), the velocity increases faster. Concerning turbulence levels, the ridge induces much higher perturbation for the flat-plate case than for the CW case. For both FP and LF configurations, the turbulence level decreases asymptotically to the initial value.

At z = 2h, observations for the FP and the LF inlet conditions are similar: the velocity decreases with increasing distance and the turbulence increases. This is the opposite behavior compared to the z = h/2 case. For the CW inlet conditions, the flow follows the same behavior as the z = h/2 case, the velocity is increasing and the turbulence intensity decreasing with increasing distance. As previously, the flow is much more affected with FP inlet conditions than with the CW.
At a distance of d = 72.h, for z = h/2, the velocity deficit is of the order of 3.4% for the FP and the LF cases, it is lower for the CW case. The relative turbulence increase is still important, especially for the FP case (+28% compare to the case without hill). At z = 2h, the velocity deficit is lower but the relative increase of turbulence much higher and very dependent on the inlet conditions.

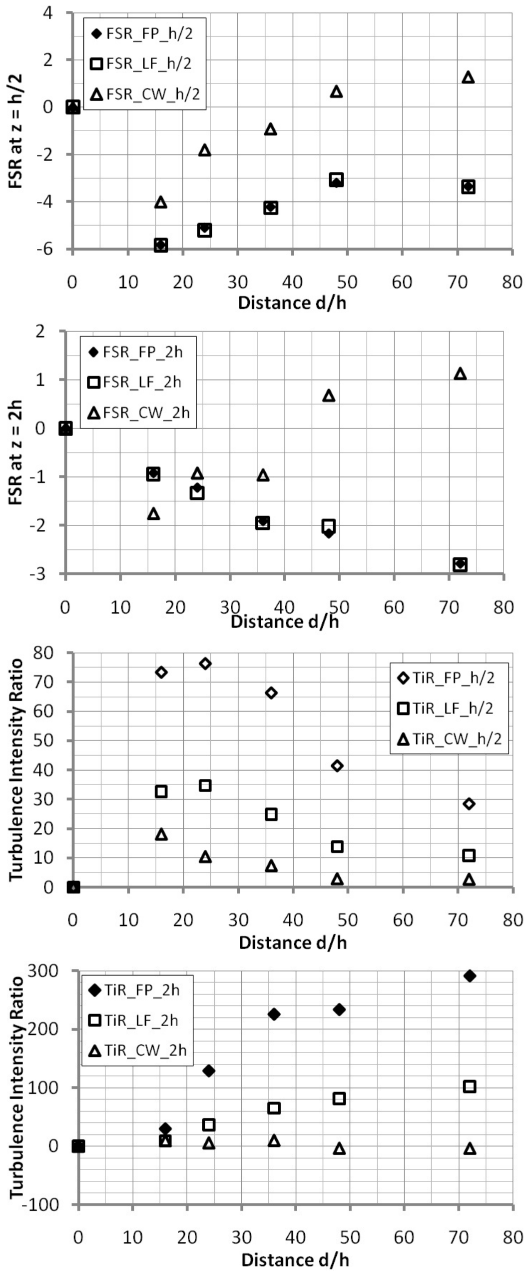

Figure 7: Fractionnal Speed-up Ratio [%] and turbulence intensity [%] evolution with the distance (FP = Flate Plate, LF = rough surface and CW = Counihan Wings).

4. Interpretation and discussions

The flow is highly affected by the ridge and a high velocity deficit is created together with a great turbulence increase. This happens at the ridge position, for z < h through a recirculation on the lee side of the ridge. After this, the flow recovers: the velocity and the turbulent level, affected by the separation, tend to come back to the inlet conditions. Flow conditions at the top of the mountain are then influenced by the distance of the ridge: the further the ridge, the more recovered is the flow when it reaches the mountain.

Above the ridge's height, the flow experiences a speed-up due to the relief, the wake propagates upward creating a velocity deficit and a turbulence

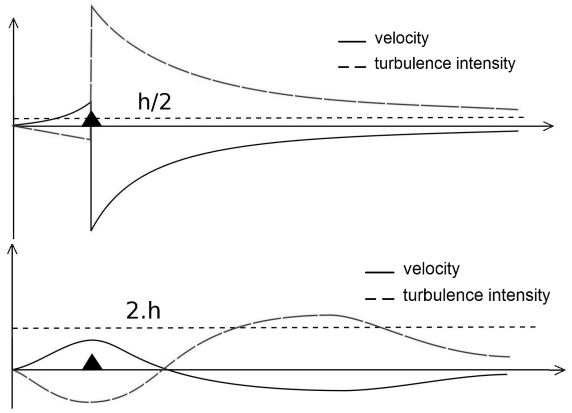

Figure 8: Tentative of a schematic representation of the evolution of the velocity and the turbulence intensity in the wake of a hill at two altitudes below and above the ridge's height.

increase for z > h. After a while, the velocity and turbulence level will then tend to come back to the inlet flow conditions. The observations are coherent with a recovery of the flow after the ridge separation (Fig.8).
From the observations, an important factor influencing the flow on the mountain's top is the inlet turbulence intensity; for the same distance, the influence of the ridge is lower for more turbulent inlet conditions. This parameter is, in this case, more important than the distance from the ridge to the mountain. The results summarized in Figure 8 presents clearly this effect: the FSR is much more affected by the inlet conditions than by the distance from the hill to the mountain. Indeed, the wake of the ridge dissipates faster in a turbulent flow.

5. Conclusions and perspectives

The study underlines the two-dimensionality of the flow around this part of the Alaiz mountain, the 1/19000 scale is a valid assumption for parametric study. However, limitation rises when reproducing the inlet conditions.
The parametric study shows the influence of the upstream ridge on the flow conditions on the top of the mountain, at 72 times the ridge height, the FSR at h/2 is influenced by -3.5% and the turbulence intensity is increased by 30% (ratio compare to inlet conditions). The turbulence is the most important quantity modified.
When changing the roughness of the inlet terrain simulated, the influence on the flow at the top of the mountain turns out to be more important than

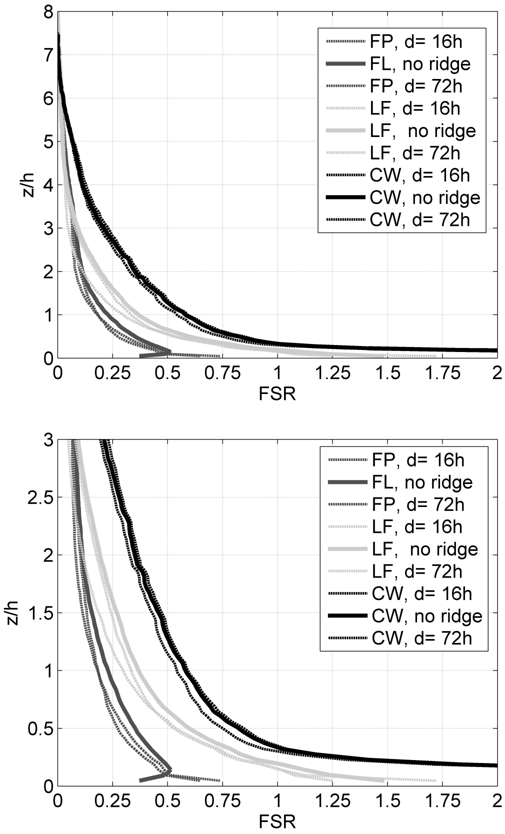

Figure 9: FSR at the mountain's top for the three inflow conditions and the two extreme ridge positions.

changing the ridge position. This is probably due to the faster wake recovery in more turbulent flows. The FSR is 37% for FP, 60% for LF and 80% for CW at h/2. The inlet condition, in this case, is a predominant parameter to consider compared to the ridge position.

For further studies, the investigation of the wake of simplified hills is planned with a particular focus on the far wake flow conditions and on the influence of the inlet flow conditions. Results can also be compared with available linear models.

Acknowledgments

This work is performed within the WAUDIT Marie-Curie Initial Training Network (Wind Resource Assessment Audit and Standardization) funded by the European Commission.
Fernando Carbajo, is greatfully acknoledge for his important participation in this work.

References

[1] J. Cermak, Applications of fluid mechanics to wind engineeringa freeman scholar lecture, Journal of Fluids Engineering 97 (1975) 9.

[2] B. Conan, S. Buckingham, , J. Van Beeck, S. Aubrun, J. Sanz, Feasibility of micro-siting in mountainous terrain by wind tunnel physical modelling, in: In: Sc. Proc. European Wind Energy Conf., March 2011, Brussels, 2011, pp. 136–140.

[3] D. Cabezón, J. Sanz, J. Van Beeck, Sensitivity analysis on turbulence models for the abl in complex terrain, in: In: Proc. Europ. Wind Energy Conf., May 2007, Milan, 2007.

[4] VDI-guidelines, Vdi guidelines 3783/12 - physical modellling of flows and dispersion processes in the atmospheric boundary layer - application of wind tunnels.

[5] D. Muñoz-Esparza, B. Conan, E. Croonenborghs, A. Parente, J. Van Beeck, J. Sanz, Sensitivity to inlet conditions of wind resourcce assessment over complex terrain using three cfd solvers and wind tunnel data, in: In: Sc. Proc. European Wind Energy Conf., March 2011, Brussels, 2011, pp. 200–204.

Mesoscale Modelling and On-site Measurements of the Offshore Boundary Layer in the North Sea

Domingo Muñoz Esparza

Environmental and Applied Fluid Dynamics Department, von Karman Institute for Fluid Dynamics, Belgium, domingo.munoz.esparza@vki.ac.be

Supervisor: Jeroen van Beeck

Professor, Environmental and Applied Fluid Dynamics Department, von Karman Institute for Fluid Dynamics, Belgium, vanbeeck@vki.ac.be

University Supervisor: Jean-Marie Buchlin

Professor, Faculté des sciences appliquées/Ecole Polytechnique, Université Libre de Bruxelles, Belgium, buchlin@vki.ac.be

Abstract

Nowadays, wind energy is increasing its contribution into the energy market. Because of that, accurate predictions of the power production are needed and thus, wind speeds need to be properly forecasted. This study thoroughly analyzes the ability of the WRF model to reprode Offshore Boundary Layer conditions under different stability scenarios. Results are validated against a comprehensive data base of field measurements from FINO1 platform, including turbulent fluxes calculated with sonic anemometry as well as LiDAR wind profiling.

Keywords: Mesoscale modelling, offshore boundary layer, turbulent fluxes, wind shear, atmospheric stability, tall wind profiles, FINO1 mast, wind energy

1. Introduction

The offshore wind capacity installed up to now in Europe is of almost 4 GW. Currently, almost 6 GW of offshore wind capacity are under construction, 17 GW have been consented by EU Member States and there are future plans for a further 114 GW. Therefore, it is expected that during this decade, offshore wind power capacity will grow tenfold to reach an estimated installed capacity of 40 GW for 2020 [1]. In order to make such a development feasible, mesoscale models play a key and promising position both for the optimization of the location of wind farms (wind resource assessment) and for the daily energy production once the wind farm will be in operation (short term forecasting).

Up to now, evaluation of wind resource assessment models at the offshore mast FINO1 was limited by the constraint in the height of the measurement mast (100 m). Nowadays, 5 MW wind turbines are typically operating in offshore wind farms, like is the case of the recently installed Alpha Ventus wind farm nearby FINO1. In that situation, the ability of mesoscale models to forecast "tall" wind profiles needs to be properly addressed as well as its applicability for wind energy purposes.

In the offshore environment, special attention has to be paid to the role of atmospheric stability. The atmospheric stability yields to notably different shear conditions and thus different velocity distributions across the rotor swept area, which dramatically influences, among others, the power production and fatigue loads on the wind turbine.

The effect of the vertical mixing due to turbulence in the planetary boundary layer (PBL) is not explicitly resolved by mesoscale models. Such models parameterize this effect employing the so-called closure techniques based on gradients of resolved quantities. For some applications, such as wind energy, where the near-surface atmospheric processes are crucial, the choice of PBL modelling becomes an important issue and thus, needs to be carefully analyzed.

In the present study, the ability of different turbulent flux parameterizations in the Weather Research

(a)

(b)

Figure 1: Research platform FINO1. (a) General view of the mast. (b) Detailed view of a sonic anemometer.

and Forecasting model (WRF-ARW) to account for the atmospheric stratification is thoroughly evaluated at FINO1. For the first time, we took advance of the recent LiDAR measurement campaign carried out at FINO1 up to 250 m height, encompassing the rotor area of the tallest wind turbines, in order to accomplish this objective. All this information allowed us to perform a complete validation based on turbulent fluxes and surface stability parameters, as friction velocity, u_*, heat flux, $< w'\theta' >$, and Obukhov length, L (derived from sonic anemometry) and on tall wind profiles measured with LiDAR.

2. Field measurements

The German research platform FINO1 is located 45 km off the Borkum Island (lat. 54○0.87'N, lon. 6○35.24'E) in the North Sea and is in operation since 2003 (Fig. 1a). In the present work, measurements from one year period (Jan. 2010 - Dec. 2010) investigated by [2] are used. Sonic anemometer data (Fig. 1b) at 40 m, 60 m and 80 m were used to derive turbulent fluxes of momentum and heat (10 Hz sampling) while slow profile response sensors (10 min averages): wind speed (cup anemometers), wind direction, relative humidity, air pressure and temperature, are mainly used for data processing.

In addition, a ground-based pulsed LiDAR system, the so-called “WindCube”, developed and manufactured by the French company Leosphere has been used in this study [3]. The LiDAR system was positioned on a container roof at approximately 10 m distance to the north-west of the offshore research mast FINO1 and performed continuous measurements from July 2009 to February 2010, scanning the wind profile up to a height of 250 m. This LiDAR has been proven to be applicable for wind speed and wind direction measurements by comparison against other velocity sensors [3; 4].

Once turbulence fluxes of heat and momentum are calculated, the atmospheric stability as described by the Monin-Obukhov Similarity Theory (MOST) was computed based on the Obukhov length, L (Eq. 1).

$$L = -\frac{\theta u_*^3}{g\kappa < w'\theta' >}, \tag{1}$$

where u_* is the friction velocity, $< w'\theta' >$ is the heat flux, g is the acceleration due to gravity, κ is the von Kármán constant (equal to 0.40) and θ is the potential temperature. Angle brackets denote ensemble averaged values.

Stability Regime	zL^{-1} [-]
Very Unstable	-4 ≤ zL^{-1} ≤ -0.2
Unstable	-0.2 < zL^{-1} ≤ -0.04
Near Neutral	-0.04 < zL^{-1} ≤ 0.04
Stable	0.04 < zL^{-1} ≤ 0.2
Very Stable	0.2 ≤ zL^{-1} ≤ 4

Table 1: Limiting values of zL^{-1} for the four stability classes in which the data is grouped (for z=40 m).

According to the values of zL^{-1}, the data has been grouped into different stability classes according to [5] (Table 1). From the developed database, long periods corresponding to each stability class has been chosen and simulated with WRF, as is shown in the upcoming sections.

3. WRF model setup

In this study we use the Numerical Weather Prediction model of the National Center for Atmospheric Research in USA (NCAR): Advance Research WRF-ARW v3.2. WRF-ARW is a conservative finite differences model that solves the unsteady non-hydrostatic compressible Euler equations [6].

Our computational domain is composed by 4 domains centered over FINO1 platform. The parent domain has a horizontal grid spacing of 27 km and covers an approximate surface of 3000 km^2, including most of Europe. Grid spacing is refined progressively by a factor of 3 through three nested domains until 1 km resolution is achieved for the most inner one, which covers approximately 100 km^2. On the vertical coordinate, 46 levels are placed. Grid spacing is of

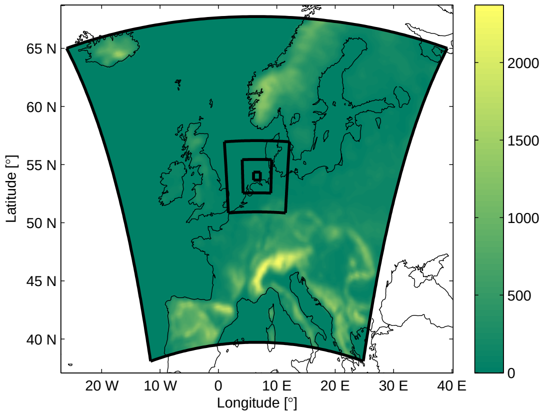

Figure 2: WRF domain configuration. The horizontal resolutions of the four domains are 27 km, 9 km, 3 km and 1 km, from the parent to the most inner domain, respectively. Color bar indicates surface elevation in meters.

10-20 m up to 300 m height to accurately resolve the lower part of the boundary layer. Above, grid spacing is progressively stretched in order to reduce the computational cost. Interactions of the meteorological fields between the domains are accounted for by two-way nesting. The domain configuration is shown in Fig. 2. The timestep is consistently reduced from the parent domain to the most inner domain in order to respect numerical stability constraints (CFL<1). WSM 3-class simple ice scheme microphysics, rapid radiative transfer in the longwave, the Dudhia shortwave scheme, NOAH surface scheme and cumulus Kain-Fritsch scheme (not applied into the two most inner domains) were used. Each PBL parameterization is tied to a particular surface layer scheme [6], all of them based on Monin-Obukhov similarity theory [7].

The parent domain is initialized and 6-hourly forced at the boundaries by meteorological fields derived from the NCEP Climate Forecast System Reanalysis data, CFSR [8], with a horizontal resolution of 0.5^{o} x 0.5^{o}. The first 24 hours are discarded as spin-up time of the model and subsequent forecasts are considered in order to devolop the proper mesoscale spectrum [9].

Previous studies have already shown that the parameterization of the vertical mixing in the PBL plays a major role on the vertical structure of the wind profile [10]. To account for that, five different PBL schemes have been tested. One first order scheme: the Yonsey University (YSU [11]), and four one-and-a-half order (or TKE closure) schemes: Mellor-Yamada-Janić (MYJ [12]), Mellor-Yamada-Nakanishi-Niino (MYNN [13]), Quasi-normal Scale Elimination (QNSE [14]) and Bougeault-Lacarrère (BouLac [15]). The differences on the order of closure are briefly described in the next section. The effect of other model parameters as: number of nested domains, horizontal resolution, physical parameterizations, etc., was investigated so the setup proposed is optimized regarding the conditions at FINO1.

4. Turbulence closure techniques

The turbulent fluxes from momentum, heat and other species in both first and one-and-a-half order closure techniques are formulated similarly [16].

$$< w'\phi' >= -K_z \left(\frac{\partial \phi}{\partial z} - \gamma \right), \tag{2}$$

where ϕ is a prognostic variable. This kind of modelization is known as gradient transport theory or K-theory. The term γ represents the non-local mixing due to larger convective eddies and it is included or not depending on the scheme. K_z is the eddy diffusivity coefficient, which sometimes has different formulations for momentum and heat. The manner in which K_z is computed introduces the differences between first and one-and-a-half orders. In first order closure techniques (YSU) the eddy diffusivities are calculated in the following way:

$$K_z(z) = \psi\left(zL^{-1}\right) \cdot z \cdot \left(1 - \frac{z}{h}\right)^2, \tag{3}$$

where h is the boundary layer height, L is the Obukhov length and $\psi\left(zL^{-1}\right)$ is a function of stability based on the nondimensional profile functions of heat and momentum [17]. The one-and-a-half order schemes solve an additional prognostic equation for the turbulent kinetic energy, q, and the parameterization of fluxes depends on q, on the master length scale, l, and on the flux Richardson number, Ri.

$$K_z(z) = \chi(Ri) \cdot l \cdot q^{0.5}. \tag{4}$$

The diagnostic equations to obtain l and $\chi(Ri)$ differ from MYJ, MYNN and QNSE. In BouLac scheme the stability function is considered as a constant coefficient.

5. Surface fluxes

In the WRF model, turbulent fluxes for momentum, heat and moisture at the surface are computed based on Monin-Obukhov Similarity Theory, as previously introduced. They represent the linkage between the surface and the atmosphere and provide lower boundary conditions for the integration of the PBL schemes. The momentum flux is parameterized based on the square of the friction velocity as showed by Eq. 5:

$$\tau_s = u_*^2 \rightarrow u_* = \frac{\kappa U_1}{\ln(z_1/z_{0m}) - \psi_m}, \tag{5}$$

where the subscript 1 stands for the conditions at the first grid point in the vertical coordinate (~10 m) and z_{0m} is the roughness length for momentum (here modeled for offshore conditions using the Charnock's equation: $z_0 = \alpha_c u_*^2/g$). Regrouping the terms from Eq. 5 it can be easily shown that the momentum flux depends on the square of the wind speed at the first grid point. For the sensible heat flux, a similar expression is used.

$$\begin{aligned} < w'\theta' >_s &= -C_H U_1 (\theta_1 - \theta_s) \\ \rightarrow C_H &= \frac{\kappa u_*}{\ln(z_1/z_{0h}) - \psi_h}, \end{aligned} \tag{6}$$

where θ_s is the sea surface temperature and z_{0h} is the roughness length for heat. In this case the parameterization of the sensible heat flux depends on the product of wind speed and the $\Delta\theta$. Furthermore, there is a dependency on the momentum flux via the surface exchange coefficient for heat C_H.

Surface fluxes of momentum and heat are compared on Fig. 3. The numerical results correspond to MYNN scheme since similar conclusions are drawn for the other PBL parameterizations. Friction velocity (Fig. 3a) is overestimated by WRF for the whole range of measurements. Indeed, a decrease on the momentum flux with height is expected when being out of the surface layer. So this effect explains the lower level of u_* measured at 40 m. In the case of sensible heat flux, WRF predicts higher values both for unstable and stable conditions. The bias is not constant anymore and it grows with $< w'\theta' >$.

In order to evaluate the ability of WRF to forecast surface stability in offshore conditions it is worthy to compare the Obukhov length. This comparison is shown in Fig. 4. Despite of the fact that similar trends were obtained for u_* and $< w'\theta' >$, combination of the two trends could produce rather different results. Under unstable atmospheric stratification (L^{-1} <0), the overestimation of both momentum and heat fluxes by the numerical model have opposite effects on L^{-1}. Simulated values of u_* tend to reduce the magnitude of L^{-1} whereas $< w'\theta' >$ contributes

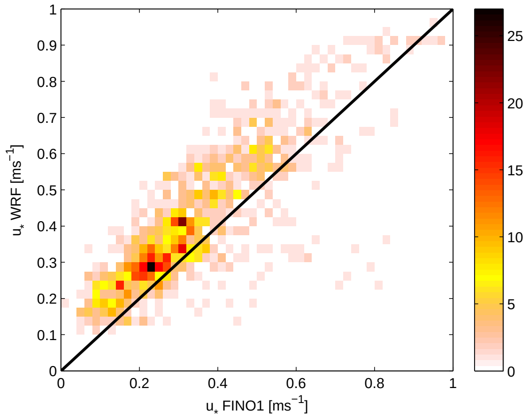

(a) Friction velocity, u_*.

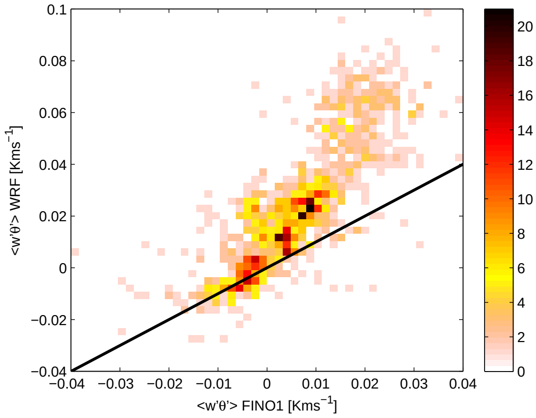

(b) Sensible heat flux, $< w'\theta' >$.

Figure 3: Two-dimensional histogram of FINO1 against WRF data (bar indicates number of data points). WRF values correspond to MYNN scheme and fluxes are 30 min averaged in all the cases.

to enhance it. For near-neutral conditions and moderate instabilities, competition of both effects yields to a slight overestimation of the inverse of the Obukhov length.

For stronger instabilities, the presence of higher values of heat flux dominates and the overestimation of L^{-1} grows. In the case of stable stability (L^{-1} >0), the values for the selected periods are lower compared to the ones measured for the convective scenarios. This gives more weight to u_* and thus, L^{-1} is underpredicted. For stable conditions the results from the five PBL parameterizations differ the most. It can be observed that QNSE (Fig. 4b) gives the best agreement with FINO1 measurements and, by contrary, BouLac (Fig. 4c) reproduce the lowest values of L^{-1}. For all the range of L^{-1} values, MYNN is the scheme which produces closer results to the field data (Fig. 4d).

In general terms, it is confirmed that WRF forecast a neutralization of the stable stratification and a reinforcement of the instability for neutral and convective stability. Those effects create a displacement of the probability density function of L^{-1} from positive towards negative values.

6. Vertical structure of the wind profile

All the numerical results presented in the previous section in terms of surface fluxes are derived from Monin-Obukhov similarity theory. For the rest of the profile, the influence of turbulent mixing on the wind speed profile is determined by the PBL tendencies, briefly described in Sec. 4. In order to analyze the performance of the PBL schemes, FINO1 profiles obtained from a combination of sonic anemometers and LiDAR data up to 250 m are considered. The obtained results are shown in Fig. 5 in terms of mean shear (referenced to the wind speed at 40 m, U_{40m}). It can be noticed that, as expected, the shear increases dramatically from very unstable conditions, in which it is much reduced or non-existing (0.2 ms^{-1} at 250 m), up to stable stratification, where the shear reaches its maximum amplitude (3.5 ms^{-1} at 250 m). Most of the time, the PBL schemes are not able to reproduce as much shear as it occurs under stable conditions. QNSE outperforms the others and BouLac and YSU produce the highest bias. The difficulties of YSU and BouLac schemes to reproduce stable profiles of wind speed are due to an excessive mixing.

This enhancing of the turbulent mixing in the lower part of the boundary layer produces a important reduction of the wind shear. This problem of the BouLac scheme is due to the assumption of constant $\chi(Ri)$ in Eq. 4. The lack of link with stability, through the Richardson number, makes it fail under stable conditions. Better agreement was found under neutral and convective conditions most probably because the coefficient is more suited for such stability regimes [10]. The failure of YSU is attributed by [10; 18] to an excessive mixing during stable stratified conditions [19]. Similar behaviour was found for YSU in onshore studies carried out by [20], forecasting neutral conditions most of the time independently on the atmospheric stability. For neutral conditions (Fig. 5b), MYNN and QNSE match the FINO1 data up to 170 m. Above, MYNN deviates slightly. Again YSU and specially BouLac schemes are the most diffusive while MYJ does not show noticeable modification from stable stratification. For the convective atmosphere (Figs. 5c-d), WRF simulations generates higher shear and the bias decreases for larger values of L^{-1}. The root-mean-square error (RMSE) of the wind shear as a function of stability has been plotted in Fig. 6. These values correspond to the average over the rotor swept area of a 5 MW wind turbine, as the ones installed in the nearby wind farm Alpha Ventus. This allows us to obtain an equivalent shear RMSE which would be "seen" by the typical wind turbines operating offshore nowadays. The results from the mean shear profiles are reflected in Fig. 6. The shear RMSE is maximum for stable conditions and shows the largest spread among the five PBL schemes. BouLac has an error of almost 1.4 ms^{-1} and QNSE and MYNN drop up to about 0.9 ms^{-1}. There is a step reduction towards neutral conditions (~0.4 ms^{-1}) with higher errors for MYJ and BouLac. In convective conditions the errors continue decreasing and reach its minimum for very unstable stability (~0.2 ms^{-1}) except for MYJ, which has the highest errors for all the unstable range and remains almost constant (~0.35 ms^{-1}).

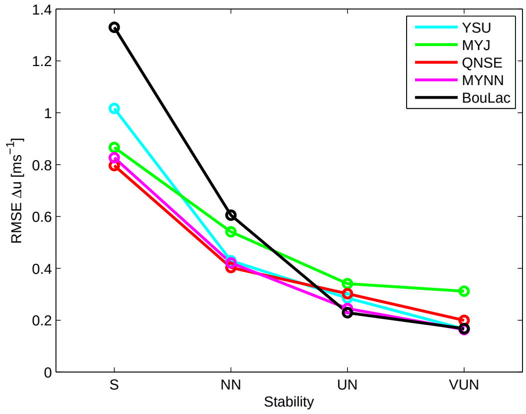

Figure 6: Averaged shear RMSE over the rotor swept area for a 5 MW wind turbine (40-160 m).

7. Conclusion

Five WRF Planetary Boundary Layer formulations were compared against field observations at FINO1 platform. Four nested domains allowed us to perform high resolution mesoscale simulations with grid spacing of 1 km in the most inner domain. Different stability scenarios were selected based on measurements of L^{-1} from the closest sonic anemometer to the surface. The observational database was composed of

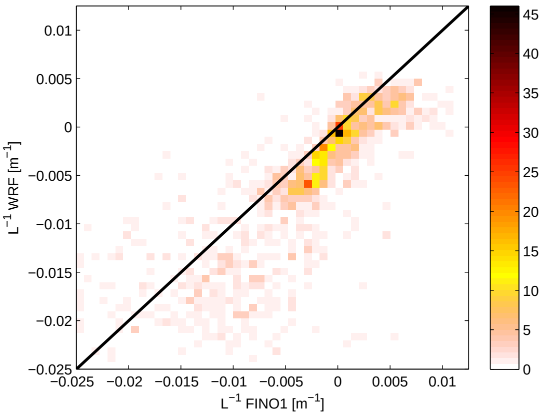

(a) YSU

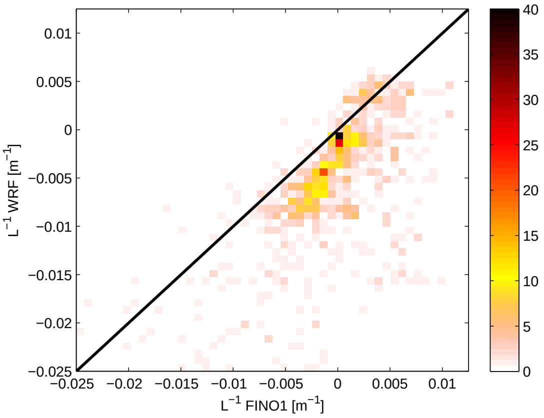

(b) QNSE

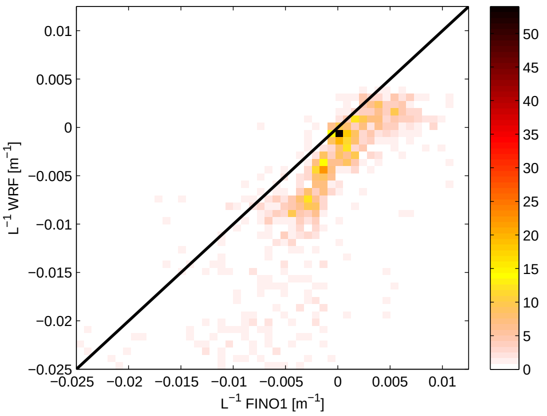

(c) BouLac

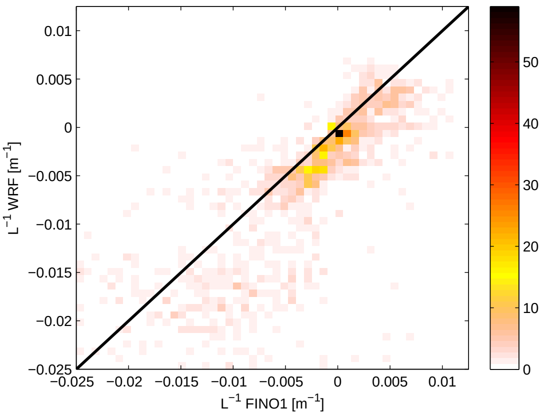

(d) MYNN

Figure 4: Two-dimensional histogram of FINO1 against WRF data for the inverse of the Obukhov length, L^{-1} (bar indicates number of data points).

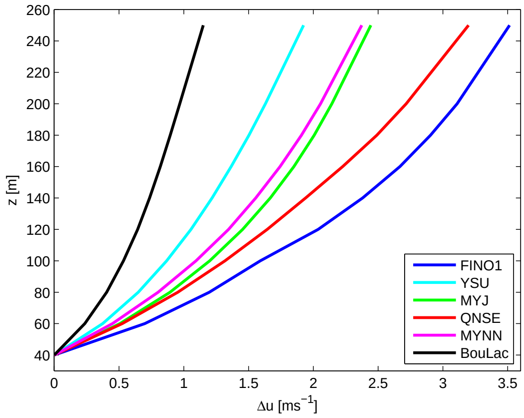

(a) Stable

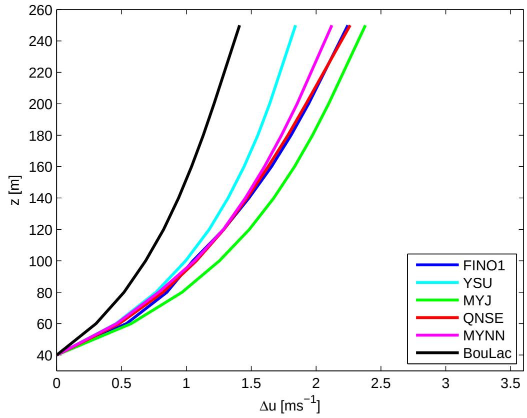

(b) Near Neutral

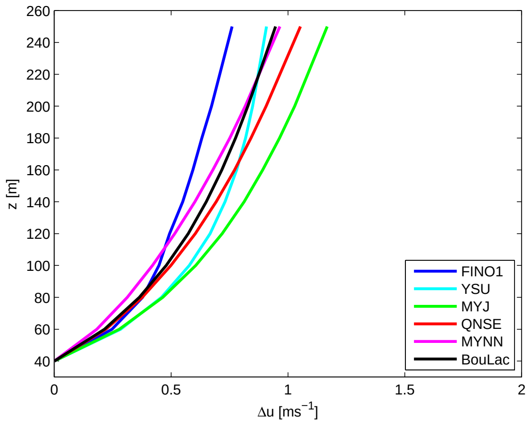

(c) Unstable

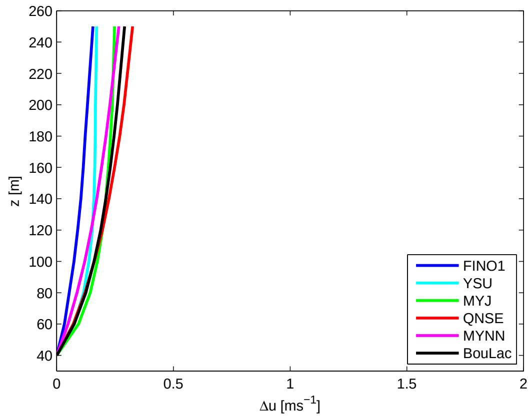

(d) Very Unstable

Figure 5: Mean wind shear profiles, $\Delta u = U - U_{40}$, grouped by stability.

combined sonic anemometers and LiDAR wind measurements in order to have both the best spatial coverage possible and including turbulent flux information.

Results concerning turbulent fluxes showed a constant overestimation of u_*. For $< w'\theta' >$ the errors are larger for higher values of $< w'\theta' >$. In terms of L^{-1}, a displacement of the probability density function of L^{-1} from positive towards negative stabilities was found.

WRF wind shear was evaluated at tall heights where 5MW WT operates and beyond, by using a LiDAR measurement campaign carried out at FINO1. In general terms, convective boundary layers present lower errors which increase with L^{-1} and with height. The shear is underestimated for stable stratification, especially for YSU and BouLac schemes, which are too diffusive.

Some differences were found between surface and profile stability indicating that vertical mixing formulation can differ from surface forcing features. From all there results here presented, we conclude that MYNN and QNSE are optimum to reproduce the offshore environment corresponding to open sea conditions for wind energy purposes, having considered surface turbulent fluxes and tall wind speed profile data for validation.

Acknowledgments

DME has been supported by the European Commission through the Marie-Curie FP7 actions under the WAUDIT project and by the Deutsches-Windenergie Institute, DEWI GmbH. DME wants to specially thank Dr. B. Cañadillas and Dr. T. Neumann for their help and support conducting this research and also to thank the hospitality of all the staff members of DEWI Wilhelmshaven during his research stay. The FINO1 platform is one of three offshore platforms of the FINO Project.

References

[1] S. Azau, Z. Casey, Wind in our sails: the coming of Europe's offshore wind energy industry, EWEA Report, European Wind Energy Association (2011).

[2] B. Cañadillas, D. Muñoz Esparza, T. Neumann, Fluxes estimation and the derivation of the atmospheric stability at the offshore mast FINO1, no. EWEA OFFSHORE 2011, Amsterdam, TheNetherlands, 2011.

[3] B. Cañadillas, A. Westerhellweg, T. Neumann, Testing the performance of a ground-based wind LiDAR system: one year intercomparison at the offshore platform FINO1, DEWI Magazine 38 (2011) 58–64.

[4] B. Cañadillas, T. Neumann, D. Muñoz Esparza, First insight in offshore wind profiles up to 250 m under free and wind turbine wake flows, no. EWEA OFFSHORE 2011, Amsterdam, TheNetherlands, 2011.

[5] A. J. M. van Wijk, A. C. M. Beljaars, A. A. M. Holtslag, W. C. Turkenburg, Evaluation of stability corrections in wind speed profiles over the North Sea, Journal of Wind Engineering and Industrial Aerodynamics 33 (1990) 551–566.

[6] W. Skamarock, J. Klemp, J. Dudhia, D. Gill, D. Barker, M. Duda, X. Huang, W. Wang, J. Powers, A description of the advanced research WRF version 3, NCAR Tech. Note NCAR/TN-475+STR, 2008.

[7] A. S. Monin, A. M. Obukhov, Basic turbulence mixing laws in the atmospheric surface layer, Tr. Inst. Teor. Geofiz. Akad. SSSR 24 (1954) 163–187. (English translation available in V. N. Bespalyi, Ed., 2001: Turbulence and Atmospheric Dynamics, J.L. Lumley, 164–194.).

[8] S. Suranjana, et. al., The NCEP Climate Forecast System Reanalysis, Bulletin of the American Meteorological Society 91 (2010) 1015–1057.

[9] W. C. Skamarock, Evaluating mesoscale NWP models using kinetic energy spectra, Monthly Weather Review 132 (2004) 3019–3032.

[10] D. Muñoz Esparza, J. van Beeck, B. Cañadillas, Impact of turbulence modelling on the performance of WRF model for offshore short-term wind energy applications, in: 13th International Conference on Wind Engineering, Amsterdam, The Netherlands, 2011.

[11] S. Y. Hong, Y. Noh, J. Dudhia, A new vertical package with an explicit treatment of entrainment processes, Monthly Weather Review 134 (2006) 2318–2341.

[12] Z. I. Janić, Nonsingular implementation of the Mellor-Yamada level 2.5 scheme in the NCEP meso model, Office Note 437, National Centers for Environmental Prediction: Camp Springs, MD, USA, 2001.

[13] M. Nakanishi, Improvement of the Meyor-Yamada turbulence closure model based on Large-Eddy Simulation data, Boundary-Layer Meteorology 99 (2001) 349–378.

[14] S. Sukoransky, B. Galperin, A. V. Perov, Application of a new spectral theory of stably stratified tur-bulence to the atmospheric boundary layer over sea ice, Boundary-Layer Meteorology 117 (2005) 231–257.

[15] P. Bougeault, P. Lacarrère, Parameterization of orography-induced turbulence in a mesobeta-scale model, Monthly Weather Review 117 (1989) 1872–1890.

[16] R. B. Stull, An introduction to boundary layer meteorology, Kluwer Academic Publishers, Dordrecht, 1988.

[17] A. J. Dyer, A review of flux-profile relationships, Boundary-Layer Meteorology 7 (1974) 363–372.

[18] B. Storm, S. Basu, The WRF model forecast-derived low-level wind shear climatology over the United States Great Plains, Energies 3 (2010) 258–276.

[19] S. Y. Hong, S. W. Kim, Stable boundary layer mixing in a vertical diffusion scheme, in: 9th WRF Users' Workshop Proceedings, Boulder, Colorado, 2008.

[20] C. Draxl, A. Hahmann, A. Peña, J. Nissen, G. Giebel, Validation of boundary-layer winds from WRF mesoscale forecasts with application to wind energy forecasting, 19th Symposium on Boundary Layer and Turbulence, Keystone, USA, 2010.